Mechanical Systems and Signal Processing 134 (2019) 106309

Contents lists available at ScienceDirect

Mechanical Systems and Signal Processing

journal homepage: www.elsevier.com/locate/ymssp

Fast iteration algorithms for implementing the acoustic beamforming of non-synchronous measurements

Liang Yu [a,b], Jerome Antoni [c], Haijun Wu [a], Quentin Leclere [c], Weikang Jiang [a,*]

[a] Institute of Vibration, Shock and Noise, State Key Laboratory of Mechanical System and Vibration, Shanghai Jiao Tong University, Shanghai 200240, China
[b] Key Laboratory of Aerodynamic Noise Control, Mianyang, Sichuan 621000, China
[c] Laboratoire Vibrations Acoustique, University of Lyon, Batiment St. Exupery 25 bis av. Jean Capelle, 69621 Villeurbanne Cedex, France

ARTICLE INFO

Article history:
Received 27 September 2018
Received in revised form 9 July 2019
Accepted 15 August 2019

Keywords:
Acoustic beamforming
Non-synchronous measurements
Augmented Lagrange multiplier (ALM) method
Alternating direction method of multipliers (ADMM)

ABSTRACT

Acoustic beamforming is a technique to measure the sound field and then achieve the localization of the sound sources. It usually works at a high frequency because the size and density of the microphone array are limited. Differing from the traditional beamforming, non-synchronous measurements beamforming can widen the working frequency bandwidth with a movable microphone array. It generates a cross-spectral matrix of all the microphones in the sequential positions of measurements, and this matrix is incomplete due to the missing phase relationships between non-synchronous measurements. Thus the non-synchronous measurements beamforming can be regarded as a cross-spectral matrix completion problem. One application of the non-synchronous measurements beamforming is that it can immediately obtain a completed noise image by scanning a large sound source; then the primary sound sources are expected to be identified by the global image. However, it is still a challenge for the current non-synchronous measurements beamforming algorithm since the computation time is long when more numbers of measurements are involved. In this paper, two algorithms based on the augmented Lagrange multiplier method and alternating direction method of multipliers are proposed for achieving fast implementation. The proposed algorithms can improve the iteration speed of the non-synchronous measurements beamforming which is proved first in the simulation, and they are further applied in the on-site measurement of the vehicle engine compartment (the data missing cross-spectral matrix of 15 non-synchronous measurements for a given frequency can be completed only in a few seconds). This industrial application has shown the potential of the proposed methods to be further applied for the sound source imaging of large mechanical systems.

1. Introduction

Acoustic imaging is widely used in the sound source identification, vibration analysis and the machine diagnosis through constructing the sound field map of the measured objects [1–3], which provided a WYSIWYG tool ("what you see is what you get") for the noise analysis. In order to achieve the acoustic imaging, two main methods including the beamforming [4–6] and Near-field Acoustical Holography (NAH) [7–9] were developed. However, the size of the microphone array and the spatial space of neighboring microphones determine respectively the lower and upper-frequency limit of the sound sources

* Corresponding author.
E-mail address: wkjiang@sjtu.edu.cn (W. Jiang).

https://doi.org/10.1016/j.ymssp.2019.106309
0888-3270/

imaging algorithms. For example, the results of the NAH are usually shown at low frequencies; the results of the beamforming are usually shown at high frequencies. Thus, the spatial distribution of the microphones in an array is the fundamental limitation for the measurement setups of the NAH and beamforming. The non-synchronous measurements [10–12] were proposed to extend the working frequency of the conventional array methods. It scans the radiating objects with a prototype microphone array, which can obtain the comparative results as a larger or denser array does. For example, the array can be virtually enlarged by moving the prototype array when the sound source is large, which generally extends the imaging results at lower frequencies; the prototype array can be virtually densified by moving an array when the sound source is small, which generally extends the imaging results at higher frequencies.

The non-synchronous measurements in the context of the NAH have been investigated as in Refs.[13–16]. For the measurements with an array of intensity probe, the non-synchronous measurements can work effectively by reconstructing the phase from the quadratic pressure and tangential components of the sound intensity [13,14,17,18]. For the measurements with an array of microphones, the non-synchronous measurements are achieved by completing a data missing cross-spectral matrix [15,16].

The initial work of non-synchronous measurements in the context of the beamforming can be found in Ref. [19]. A fast and robust implementation of the cross-spectral matrix completion is essential for the acoustic beamforming, whereas a high accuracy implementation of cross-spectral matrix completion is more important for the NAH. The different challenges of computational efficiency and accuracy will result in a various selection of nuclear norm minimization algorithms. Especially in practice, a fast implementation of non-synchronous measurements beamforming is usually helpful to approximately know the sources positions and relative strength for a very large object of testing, which is un-achievable for the conventional beamforming and its variant. Thus, two fast algorithms that are based on the augmented Lagrange multiplier (ALM) and alternating direction method of multipliers (ADMM) are proposed in this paper. The proposed methods can rapidly obtain an approximate image of the sound field in the on-site measurement. If the sound field is required to be further quantified for the local area of the large object, the aperture-focused NAH methods (for example, using a designed mask [20] to cover the approximate sound sources or selecting an appropriate aperture function in the Bayesian focusing [21]) may be further applied with the known sources positions that are estimated by aforementioned step of the non-synchronous measurements beamforming.

The paper is organized as follows. The forward model of non-synchronous measurements beamforming is described in Section 2, and the cross-spectral matrix completion with nuclear norm minimization is given in Section 3. Faster algorithms are introduced in Section 4 and Section 5, and the simulations are given in Section 6. Section 7 provides an industrial application of the engine compartment on-site measurements and Section 8 is the conclusion.

2. Forward model of non-synchronous measurements beamforming

S incoherent broadband sound sources are assumed to distributed discretely on a plane which is divided into N grids, and M microphones are set to measure these sound sources ($N > M > S$). Then measured pressures $\mathbf{p}_t = (p_1, \ldots, p_M)_t^T$ can be obtained with many snapshots (Fourier Transform of a short-time segment [19]), that is

$$\mathbf{p}_t = \mathbf{G}(r)\mathbf{s}_t + \mathbf{n}_t, \tag{1}$$

where $\mathbf{s}_t = (s_1, \ldots, s_S)_t^T$ represents the amplitudes of the sound sources and $\mathbf{n}_t = (n_1, \ldots, n_M)_t^T$ is assumed to be the measurement noise which is complex Gaussian distributed with 0-mean and β^2-covariance. $(\cdot)^T$ is the symbol of transpose and t represents the t-th snapshot. A free-field propagation is assumed, with Green's function matrix $\mathbf{G}(r)$ written as

$$\mathbf{G}(r) = \begin{bmatrix} g_{1,1} & & & \\ & \ddots & & \\ & & g_{m,s} & \\ & & & \ddots \end{bmatrix}_{M\times S}, \quad g_{m,s} = \frac{e^{jk_w\|\mathbf{r}_m - \mathbf{r}_s\|}}{4\pi\|\mathbf{r}_m - \mathbf{r}_s\|}. \tag{2}$$

Here, k_w is the wave-number and j is the symbol for imaginary numbers. $\mathbf{r}_m, m = 1, \ldots, M$ is the location of the microphones and $\mathbf{r}_s, s = 1, \ldots, S$ is the coordinates of sound sources. Besides, it is worthwhile to notice that $\mathbf{n}_t$ and $\mathbf{s}_t$ are independent. Thus, the corresponding cross-spectral matrix of propagation can be obtained as follows [19].

$$\mathbf{S}_{pp} = \mathbb{E}\{\mathbf{p}_t\mathbf{p}_t^H\} = \mathbb{E}\left\{\mathbf{G}\mathbf{s}_t\mathbf{s}_t^H\mathbf{G}^H + \mathbf{n}_t\mathbf{n}_t^H\right\} = \mathbf{G}\mathrm{diag}(\boldsymbol{\alpha}^2)\mathbf{G}^H + \beta^2\mathbf{I}_M, \tag{3}$$

where $\mathbb{E}\{\cdot\}$ denotes the mathematical expectation; $(\cdot)^H$ is the conjugate transpose and $\boldsymbol{\alpha}^2 = (\alpha_1^2, \ldots, \alpha_S^2)^T$ is the vector of sound source powers (variances of amplitudes). $\mathbf{I}_M$ is the $M \times M$ identity matrix and $\mathrm{diag}(\boldsymbol{\alpha}^2)$ is the square diagonal matrix with the l-th diagonal entry being $\alpha_l^2, l = 1, \ldots, S$.

When the model of non-synchronous measurements is constructed, the i-th measurement of non-synchronous microphone array measurements has the form

$$\mathbf{p}_t^{\{i\}} = \mathbf{G}^{\{i\}}(r)\mathbf{s}_t + \mathbf{n}_t^{\{i\}}, \tag{4}$$

where $i = 1, \ldots, P$ and P is the number of non-synchronous measurements. Then, the corresponding cross-spectral matrix is

$$\mathbf{S}_{pp}^{(i)} = \mathbb{E}\left\{\mathbf{p}_t^{\{i\}}\mathbf{p}_t^{\{i\}H}\right\} = \mathbf{G}^{\{i\}}\mathrm{diag}(\boldsymbol{\alpha}^2)\mathbf{G}^{\{i\}H} + \beta_i^2\mathbf{I}_M, \quad 1, \ldots, P. \tag{5}$$

According to Welch's method [22], Eq. (5) can be estimated by $\hat{\mathbf{S}}_{pp}^{(i)} = \frac{1}{t_T}\sum_{t=1}^{t_T}\mathbf{p}_t^{\{i\}}\mathbf{p}_t^{\{i\}H}$, where t_T denotes the number of snapshots. The cross-spectral matrix $\hat{\mathbf{S}}_{pp}$ of simultaneous measurement is a full matrix with the size $MP \times MP$, and each sub-matrix $\hat{\mathbf{S}}_{pp}^{(i)}$ of non-synchronous measurements has a dimension of $M \times M$ which is shown in Fig. 1. The problem of non-synchronous measurements boils down to a matrix completion problem, and the only known information is the sub-matrices $\hat{\mathbf{S}}_{pp}^{(i)}, i = 1, \ldots, P$ which is located on the diagonal positions of an incomplete cross-spectral matrix $\hat{\mathbf{S}}_{pp}^{m}$. Then a virtual MP microphone array can be obtained by moving a M microphone array P times.

3. Cross-spectral matrix completion with nuclear norm minimization

Based on the discussion in Section 2, the problem is reformulated as follows to seek a full cross-spectral matrix $\mathbf{S} \in \mathbb{C}^{MP\times MP}$ from the matrix $\hat{\mathbf{S}}_{pp}^{m} \in \mathbb{C}^{MP\times MP}$ of data missing, which can be solved by the gradient algorithms such as Fast Iterative Shrinkage Thresholding Algorithm (FISTA) [16].

$$\underset{\mathbf{S}}{\text{minimize}}\ \|\mathbf{S}\|_* \text{subject to} \|\mathcal{A}(\mathbf{S}) - \hat{\mathbf{S}}_{pp}^{m}\|_F \leqslant \epsilon; \|\boldsymbol{\Psi}\mathbf{S}\boldsymbol{\Psi}^H - \mathbf{S}\|_F \leqslant \varepsilon; \mathbf{S}^H = \mathbf{S} \succeq 0. \tag{6}$$

In Eq. (6), $\|\cdot\|_*$ denotes the nuclear norm, $\|\cdot\|_F$ represents the Frobenius norm and $\mathcal{A}: \mathbb{C}^{MP\times MP} \to \mathbb{C}^{MP\times MP}$ is a sampling operator that extracts the element from diagonal blocks. Specifically, the following constraints are added here to make the structured low rank model more feasible. $\|\mathcal{A}(\mathbf{S}) - \hat{\mathbf{S}}_{pp}^{m}\|_F \leqslant \epsilon$ is imposed to express the relation between the object matrix $\mathbf{S}$ and the incomplete matrix $\hat{\mathbf{S}}_{pp}^{m}$, where the given tolerance ϵ is the estimation and measurement error. $\|\boldsymbol{\Psi}\mathbf{S}\boldsymbol{\Psi}^H - \mathbf{S}\|_F \leqslant \varepsilon$ is enforced to ensure spatial continuity of the acoustic field, where $\boldsymbol{\Psi} \in \mathbb{C}^{MP\times MP}$ is a projection basis proposed in Ref. [10] and ε is the representation error. Besides, the Hermitian and positive semi-definite property is an inherent characteristic of the spectral matrix, so $\mathbf{S} \succeq 0$ should be satisfied and $\mathbf{S}$ should also be equal to $\mathbf{S}^H$. In the following sections, two methods based on the augmented Lagrange multiplier method and alternating direction method of multipliers are proposed to solve the optimization problem of Eq. (6).

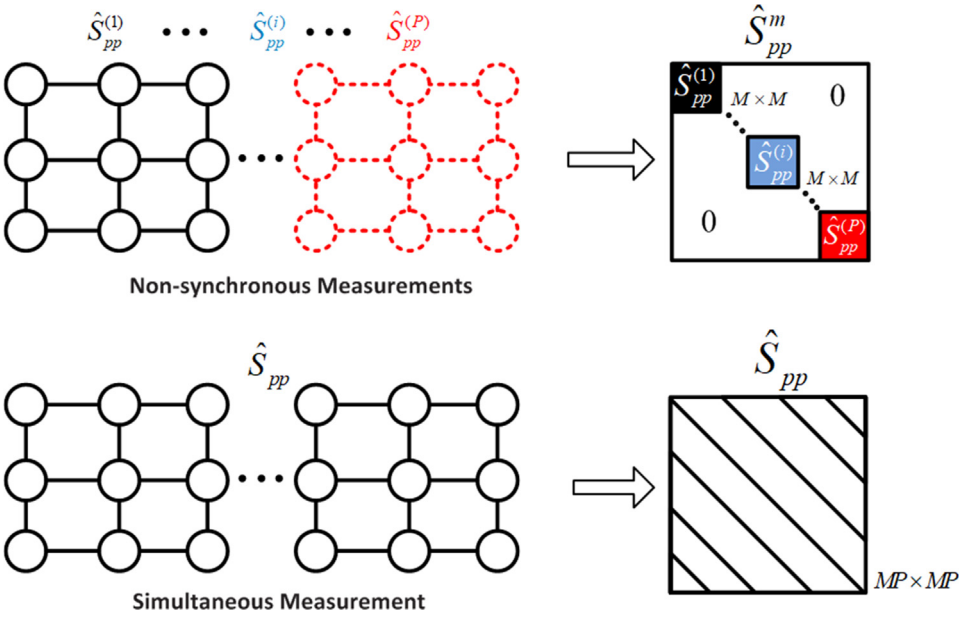

Fig. 1. Measurement mode and cross-spectral matrix: non-synchronous measurements (upside) versus simultaneous measurement (downside).

4. Augmented Lagrange multiplier algorithm

4.1. The theory of ALM algorithm

In order to solve the optimization problem of Eq. (6), the general augmented Lagrange multiplier method is introduced in this subsection. It is a certain class of algorithms for solving constrained optimization problems, which reformulates the constrained optimization problem as the unconstrained problems. Specifically, it adds a term designed to represent the Lagrange multiplier and the penalty term. The general augmented Lagrange multiplier method is offered for solving problems which reads [23]

$$\text{minimize } f(X) \quad \text{subject to} \quad h(X) = 0, \tag{7}$$

where $f : \mathbb{R}^{n'} \to \mathbb{R}, h : \mathbb{R}^{n'} \to \mathbb{R}^{m'}$, and m' and n' denote positive integers which are different from m and n used in Section 2. Then the augmented Lagrangian function can be defined as

$$L(X, Y, \mu) = f(X) + \langle Y, h(X)\rangle + \frac{\mu}{2}\|h(X)\|_F^2, \tag{8}$$

where μ is a positive penalty parameter, Y is a Lagrange multiplier and $\langle\rangle$ denotes the inner product. It is well known that the above optimization problem can be solved by following iteration steps, and the procedure of computation is further formulated in Algorithm 1 [24].

$$X_{k+1} = \underset{X}{\operatorname{argmin}} \quad L(X, Y_k, \mu_k); \tag{9}$$

$$Y_{k+1} = Y_k + \mu_k h(X_{k+1}). \tag{10}$$

The convergence of the algorithm depends on the sequence μ_k (Q-linear when μ_k is bounded and super-Q-linear when μ_k is unbounded).

Algorithm 1 (General Iterations of ALM Algorithm)

1: $\rho \geqslant 1$ (ρ is a scale factor).
2: **When** not converged **do**
3: Solve $X_{k+1} = \arg\min_X L(X, Y_k, \mu_k)$;
4: $Y_{k+1} = Y_k + \mu_k h(X_{k+1})$;
5: $\mu_{k+1} = \rho\mu_k$;
6: **End**
7: Output: X_{k+1}.

4.2. Non-synchronous measurements by augmented Lagrange multiplier algorithm

As shown in Eq. (6), the non-synchronous measurements problem can be viewed as a constrained optimization problem

$$\underset{\mathbf{S}}{\text{minimize}} \ \|\mathbf{S}\|_* \quad \text{subject to} \quad \mathbf{S} + \mathbf{E} = \widehat{\mathbf{S}}_{pp}^m; \quad \mathcal{A}(\mathbf{E}) = 0, \tag{11}$$

where the matrix $\mathbf{E}$ is given to compensate for the matrix $\widehat{\mathbf{S}}_{pp}^m$ which can be constructed as follows.

$$\text{construct } \mathbf{E} \text{ with } [\mathbf{E}]_{i'j'} = \begin{cases} -[\mathbf{S}]_{i'j'} & i'j' \notin \Upsilon; \\ 0 & i'j' \in \Upsilon. \end{cases}$$

Here, Υ denotes the position set of fixed diagonal block in the matrix $\widehat{\mathbf{S}}_{pp}^m$, which is shown in Fig. 1 and $[]_{i'j'}$ denotes the (i', j') element of the matrix $\mathbf{S}$. Thus its augmented Lagrange function can be written as

$$L(\mathbf{S}, \mathbf{E}, \mathbf{Y}, \mu) = \|\mathbf{S}\|_* + \left\langle \mathbf{Y}, \widehat{\mathbf{S}}_{pp}^m - \mathbf{S} - \mathbf{E} \right\rangle + \frac{\mu}{2}\|\widehat{\mathbf{S}}_{pp}^m - \mathbf{S} - \mathbf{E}\|_F^2, \tag{12}$$

where $\mathbf{Y} \in \mathbb{C}^{MP\times MP}$ is a Lagrange multiplier and μ is a penalty parameter. Besides, $\|\boldsymbol{\Psi}\mathbf{S}\boldsymbol{\Psi}^H - \mathbf{S}\|_F \leqslant \varepsilon$ should be enforced by setting $\mathbf{S} = \boldsymbol{\Psi}\mathbf{S}\boldsymbol{\Psi}^H$ in each iteration and a stopping criterion is taken into consideration,

$$\|\widehat{\mathbf{S}}_{pp}^m - \mathbf{S}_k - \mathbf{E}_k\|_F / \|\widehat{\mathbf{S}}_{pp}^m\|_F < \varepsilon_1, \tag{13}$$

where $\mathbf{E}_k = \bar{\mathcal{A}}\left(\widehat{\mathbf{S}}_{pp}^m - \mathbf{S}_k + \mu_{k-1}^{-1}\mathbf{Y}_{k-1}\right) = \mathcal{A}(\mathbf{S}_k) - \mathbf{S}_k, \bar{\mathcal{A}} : \mathbb{C}^{MP\times MP} \to \mathbb{C}^{MP\times MP}$ is a sampling operator that extracts the elements from non-diagonal blocks and ε_1 is a constant parameter chosen by the user. μ is set to be a non-zero constant in this paper, and the non-synchronous measurements problem can be solved with the ALM algorithm which is shown in Algorithm 2 (see Appendix A for the derivation of the main iteration steps). In this algorithm, the operator shrink is calculated as

$\mathbf{U}_k\mathrm{diag}(\max\{\boldsymbol{\sigma}_k-\boldsymbol{\mu},\mathbf{0}\})\mathbf{U}_k^H$, where $\boldsymbol{\sigma}_k=(\sigma_{k_1},\ldots,\sigma_{k_{MP}})^T,\boldsymbol{\mu}=(\mu,\ldots,\mu)^T,\mathbf{0}=(0,\ldots,0)^T$ are all $MP\times 1$ vectors and $\max\{\boldsymbol{\sigma}_k-\boldsymbol{\mu},\mathbf{0}\}$ takes the maximum value at the same entry of vector $\boldsymbol{\sigma}_k-\boldsymbol{\mu}$ and $\mathbf{0}$ to form a new vector. Specifically, $\mathbf{U}_k\mathrm{diag}(\boldsymbol{\sigma}_k)\mathbf{U}_k^H=\mathbf{G}_k$ is the Eigenvalue Decomposition (EVD) of the matrix $\mathbf{G}_k$, where $\mathrm{diag}(\boldsymbol{\sigma}_k)$ is the eigenvalue matrix and $\mathbf{U}_k$ is the matrix composed of corresponding eigenvectors.

Algorithm 2 (Non-synchronous Measurements with the ALM Algorithm)

1: Starts with $\mathbf{Y}_1=\mathbf{E}_1=\mathbf{0}\in\mathbb{C}^{MP\times MP}$ (zero matrix); the data missing cross-spectral matrix is $\widehat{\mathbf{S}}_{pp}^m$ and μ is a given penalty parameter.
2: **For**$k=1:N_m$ (N_m is the maximum iteration steps)
3: $\mathbf{G}_k=\widehat{\mathbf{S}}_{pp}^m-\mathbf{E}_k+\mu^{-1}\mathbf{Y}_k$;
4: $\tilde{\mathbf{S}}_k=\mathrm{shrink}(\mathbf{G}_k,\mu)$;
5: $\mathbf{S}_{k+1}=\boldsymbol{\Psi}\tilde{\mathbf{S}}_k\boldsymbol{\Psi}^H$;
6: $\mathbf{E}_{k+1}=\bar{\mathcal{A}}\left(\widehat{\mathbf{S}}_{pp}^m-\mathbf{S}_{k+1}+\mu^{-1}\mathbf{Y}_k\right)$;
7: $\mathbf{Y}_{k+1}=\mathbf{Y}_k+\mu\left(\widehat{\mathbf{S}}_{pp}^m-\mathbf{S}_{k+1}-\mathbf{E}_{k+1}\right)$;
8: **If** Stopping criterion $\leqslant\varepsilon_1$,
9: **break**
10: **End if**
11: **End**
12: Output $\mathbf{S}_{k+1}$ (full cross-spectral matrix).

5. Alternative direction method of multipliers algorithm

5.1. The theory of ADMM algorithm

The alternating direction method of multipliers algorithm which combines the dual ascent and the method of multipliers is presented here to solve the non-synchronous measurements problem. Generally, it is suitable for solving the problems offered in Refs. [25,26], that is

$$\begin{aligned}&\text{minimize}\quad f(X)+g(Z)\\&\text{subject to}\quad \mathbf{A}X+\mathbf{B}Z=C,\end{aligned}\tag{14}$$

where $X\in\mathbb{R}^{n'},Z\in\mathbb{R}^{m'},\mathbf{A}\in\mathbb{R}^{q\times n'},\mathbf{B}\in\mathbb{R}^{q\times m'},C\in\mathbb{R}^q,q$ is a positive integer and $g:\mathbb{R}^{m'}\to\mathbb{R}$. Then its augmented Lagrangian function can be formed as

$$L_\mu(X,Z,Y)=f(X)+g(Z)+\langle Y,\mathbf{A}X+\mathbf{B}Y-C\rangle+(\mu/2)\|\mathbf{A}X+\mathbf{B}Y-C\|_F^2,\tag{15}$$

where μ is a positive penalty parameter and Y is a Lagrange multiplier. The iterations of ADMM consist of three steps

$$X_{k+1}=\underset{X}{\operatorname{argmin}}\quad L_\mu(X,Z_k,Y_k);\tag{16}$$

$$Z_{k+1}=\underset{Z}{\operatorname{argmin}}\quad L_\mu(X_{k+1},Z,Y_k);\tag{17}$$

$$Y_{k+1}=Y_k+\mu(\mathbf{A}X_{k+1}+\mathbf{B}Z_{k+1}-C).\tag{18}$$

Therefore, the optimization problem as Eq. (14) can be solved by Algorithm 3 and a review of the convergence analysis can be found in Ref. [27].

Algorithm 3 (General Iterations of ADMM Algorithm)

1: **While** not converged **do**
2: Solve $X_{k+1}=\arg\min_X L(X,Z_k,Y_k)$;
3: Solve $Z_{k+1}=\arg\min_Z L(X_{k+1},Z,Y_k)$;
4: $Y_{k+1}=Y_k+\mu(\mathbf{A}X_{k+1}+\mathbf{B}Z_{k+1}-C)$;
5: **End**
6: Output: X_{k+1}

5.2. Non-synchronous measurements by alternating direction method of multipliers algorithm

In order to solve the non-synchronous measurements problem with the ADMM algorithm, Eq. (6) should be reformulated with the nuclear norm regularized linear least squares form as follows.

$$\underset{\mathbf{S}}{\text{minimize}}\ \lambda\|\mathbf{S}\|_* + \frac{1}{2}\|\mathcal{A}(\mathbf{S}) - \widehat{\mathbf{S}}_{pp}^m\|_F^2 \quad \text{subject to} \quad \mathbf{S} \succeq 0, \tag{19}$$

where λ is a regularization parameter that balances the cross-spectral matrix fitting term and the regularization term. Besides, a new matrix variable $\mathbf{M}$ is offered and an equivalent form of Eq. (19) can be obtained,

$$\underset{\mathbf{S},\mathbf{M}}{\text{minimize}}\ \lambda\|\mathbf{S}\|_* + \frac{1}{2}\|\mathcal{A}(\mathbf{M}) - \widehat{\mathbf{S}}_{pp}^m\|_F^2 \quad \text{subject to} \quad \mathbf{S} = \mathbf{M}, \quad \mathbf{S} \succeq 0. \tag{20}$$

Then its augmented Lagrangian function is

$$L(\mathbf{S},\mathbf{M},\mathbf{Y}) = \lambda\|\mathbf{S}\|_* + \frac{1}{2}\|\mathcal{A}(\mathbf{M}) - \widehat{\mathbf{S}}_{pp}^m\|_F^2 + \langle \mathbf{Y}, \mathbf{S} - \mathbf{M}\rangle + \frac{\mu}{2}\|\mathbf{S} - \mathbf{M}\|_F^2, \tag{21}$$

where $\mathbf{Y} \in \mathbb{C}^{MP\times MP}$ is a Lagrange multiplier, and μ is a positive penalty parameter. According to Eqs. (16)–(18), the ADMM algorithm of non-synchronous measurements updates $\mathbf{S}$ and $\mathbf{M}$ alternatively in the form

$$\mathbf{S}_{k+1} = \arg\min_{\mathbf{S}\succeq 0} \quad L_\mu(\mathbf{S},\mathbf{M}_k,\mathbf{Y}_k); \tag{22}$$

$$\mathbf{M}_{k+1} = \arg\min_{\mathbf{M}} \quad L_\mu(\mathbf{S}_{k+1},\mathbf{M},\mathbf{Y}_k); \tag{23}$$

$$\mathbf{Y}_{k+1} = \mathbf{Y}_k + \gamma\mu(\mathbf{S}_{k+1} - \mathbf{M}_{k+1}), \tag{24}$$

where γ is a relaxation parameter [28].

With the operator shrink mentioned in Algorithm 2, Eq. (22) can be further written as

$$\mathbf{S}_{k+1} = \mathbf{U}_k \mathrm{diag}(\max\{\boldsymbol{\omega}_k - \boldsymbol{\lambda}/\boldsymbol{\mu}, \mathbf{0}\})\mathbf{U}_k^H, \tag{25}$$

where $\mathbf{U}_k$ and $\mathrm{diag}(\boldsymbol{\omega}_k)$ are respectively the eigenvector matrix and eigenvalue matrix of the matrix $\mathbf{M}_k - (1/\mu)\mathbf{Y}_k$, and $\boldsymbol{\lambda} = (\lambda,\ldots,\lambda)^T$ and $\boldsymbol{\omega}_k = (\omega_{k_1},\ldots,\omega_{k_{MP}})^T$ are $MP\times 1$ vectors. Eqs. (23) and (24) can be further written as follows (see Appendix B for the derivation of the main iteration steps).

$$\mathcal{A}(\mathbf{M}_{k+1}) = \frac{1}{\mu+1}\mathcal{A}\left(\widehat{\mathbf{S}}_{pp}^m + \mu\mathbf{S}_{k+1} + \mathbf{Y}_k\right); \tag{26}$$

$$\bar{\mathcal{A}}(\mathbf{M}_{k+1}) = \bar{\mathcal{A}}(\mathbf{S}_{k+1} + (1/\mu)\mathbf{Y}_k); \tag{27}$$

$$\mathbf{Y}_{k+1} = \mathbf{Y}_k + \gamma\mu(\mathbf{S}_{k+1} - \mathbf{M}_{k+1}). \tag{28}$$

Correspondingly, the stopping criterion of the ADMM algorithm of the non-synchronous measurements is

$$\|\mathcal{A}(\mathbf{S}) - \hat{\mathbf{S}}_{pp}^m\|_F / \|\hat{\mathbf{S}}_{pp}^m\|_F \leqslant \varepsilon_2, \tag{29}$$

where ε_2 is a convergence tolerance chosen by the user. $\|\boldsymbol{\Psi}\mathbf{S}\boldsymbol{\Psi}^H - \mathbf{S}\|_F \leqslant \varepsilon$ should also be enforced by setting $\mathbf{S} = \boldsymbol{\Psi}\mathbf{S}\boldsymbol{\Psi}^H$ in each iteration. Therefore, the non-synchronous measurements problem can be solved by the ADMM algorithm which is shown in Algorithm 4.

Algorithm 4 (Non-synchronous Measurements with the ADMM Algorithm)

1: Starts with $\mathbf{Y}_1 = 0 \in \mathbb{C}^{MP\times MP}$, randomly assigned matrix $\mathbf{M}_1 \in \mathbb{C}^{MP\times MP}$ and input matrix $\widehat{\mathbf{S}}_{pp}^m$. μ,γ and λ are given parameters.
2: **For** $k = 1 : N_m$ (N_m is the maximum iteration steps)
3: $\mathbf{G}_k = \mathbf{M}_k - (1/\mu)\mathbf{Y}_k$;
4: $\tilde{\mathbf{S}}_k = \mathrm{shrink}(\mathbf{G}_k, \lambda/\mu)$;
5: $\mathbf{S}_{k+1} = \boldsymbol{\Psi}\tilde{\mathbf{S}}_k\boldsymbol{\Psi}^H$;
6: $\mathbf{E}_k = \mathbf{S}_{k+1} + (1/\mu)\mathbf{Y}_k$;
7: $\mathcal{A}(\mathbf{M}_{k+1}) = 1/(\mu+1)\mathcal{A}\left(\widehat{\mathbf{S}}_{pp}^m + \mu\mathbf{E}_k\right)$;
8: $\bar{\mathcal{A}}(\mathbf{M}_{k+1}) = \bar{\mathcal{A}}(\mathbf{E}_k)$;
9: $\mathbf{Y}_{k+1} = \mathbf{Y}_k + \gamma\mu(\mathbf{S}_{k+1} - \mathbf{M}_{k+1})$;
10: **If** Stopping criterion $\leqslant \varepsilon_2$,
11: **break**
12: **End for if**
13: **End**
14: Output $\mathbf{S}_{k+1}$ (full cross-spectral matrix).

6. Simulation results

In this section, several simulations are run to validate the proposed beamforming methods based on a different number of non-synchronous measurements under various scenarios. First, a prototype array with 21 microphones for the non-synchronous measurements is shown in Fig. 2. The measurement distance between the microphone array and the source plane in the z-axis direction is set to be 1 m. The source plane (length 1 m and width 1 m) is discretized uniformly by 21×21 grids (with mesh grid 0.1 m), and two point sound sources located separately at (0.3 0 1) (−0.3 0 1) (meters) are simulated to generate the acoustic field. It should be noted that the two sound sources can not be resolved (distinguished) for the current setting with only the prototype array due to the poor resolution of such a small array (for the definition of array resolution can be found in Ref. [29,30]). This can be shown in Fig. 3: the two sound sources in the beamforming results of the prototype array can not be resolved at 3000 Hz and the aliasing happens at 5000 Hz (and its beyond frequencies). Thus, the non-synchronous measurements beamforming is considered to increase the resolution. The central positions of different numbers of non-synchronous measurements are set as follows.

1. 4 non-synchronous measurements: (−0.05 −0.05 0), (−0.05 0.05 0), (0.05 −0.05 0), (0.05 0.05 0) (meters).
2. 9 non-synchronous measurements: (−0.05 −0.05 0), (−0.05 0.01 0), (−0.05 0.05 0), (0.01 −0.05 0), (0.01 0.01 0), (0.01 0.05 0), (0.05 −0.05 0), (0.05 0.01 0), (0.05 0.05 0) (meters).
3. 16 non-synchronous measurements: (−0.05 −0.05 0), (−0.05 −0.03 0), (−0.05 0.03 0), (−0.05 0.05 0), (−0.03 −0.05 0), (−0.03 −0.03 0), (−0.03 0.03 0), (−0.03 0.05 0), (0.03 −0.05 0), (0.03 −0.03 0), (0.03 0.03,0), (0.03 0.05 0), (0.05 −0.05 0), (0.05 −0.03 0), (0.05 0.03 0), (0.05 0.05 0) (meters).
4. 25 non-synchronous measurements: (−0.05 −0.05 0), (−0.05 −0.03 0), (−0.05 0.01 0), (−0.05 0.03 0), (−0.05 0.05 0) (−0.03 −0.05 0), (−0.03 −0.03 0), (−0.03 0.01 0), (−0.03 0.03 0), (−0.03 0.05 0), (0.01 −0.05 0), (0.01 −0.03 0), (0.01 0.01 0), (0.01 0.03 0), (0.01 0.05 0), (0.03 −0.05 0), (0.03 −0.03 0), (0.03 0.01 0), (0.03 0.03 0), (0.03 0.05 0), (0.05 −0.05 0), (0.05 −0.03 0), (0.05 0.01 0), (0.05 0.03 0), (0.05 0.05 0) (meters).

The data missing cross-spectral matrices of 4, 9, 16 and 25 non-synchronous measurements are respectively shown in Fig. 4(a)–(d). The completion of the data missing cross-spectral matrix is a difficult issue since the known elements of each number of non-synchronous measurements are only 25%, 11%, 6% and 4%.

A complex Gaussian noise with SNR = 10 dB, SNR = 20 dB, SNR = 30 dB and SNR = 60 dB is separately added to 100 snapshots of sound pressures to produce the measured pressures (in the frequency domain), and the spectral matrices of the simultaneous measurements (full matrix) and non-synchronous measurements (incomplete matrix) are separately estimated. The cross-spectral matrix completion error (MCE) is viewed as a criterion for the quality of cross-spectral matrix completion, which is calculated as

$$\mathrm{MCE} = \frac{\|\mathbf{S}_{pp}^{\{sim\}} - \mathbf{S}_{pp}^{\{com\}}\|_F}{\|\mathbf{S}_{pp}^{\{sim\}}\|_F}, \tag{30}$$

where $\mathbf{S}_{pp}^{\{sim\}}$ is the simulated cross-spectral matrix and $\mathbf{S}_{pp}^{\{com\}}$ is the completed cross-spectral matrix.

The parameters of FISTA [16] are chosen as follows: maximum iteration for each regularization step $N_m = 2$, stopping criterion $\mathrm{SC} = 1e-2$, initial regularization parameter $\lambda_0 = \|\hat{\mathbf{S}}_{pp}^m\|_F$, final regularization parameter $\lambda_d = 10^{-2}\lambda_0$ and step size $\mu = 1.2$. The parameters for ALM are chosen as follows: maximum iteration step $N_m = 2$, stopping criterion $\varepsilon_1 = 1e-2$,

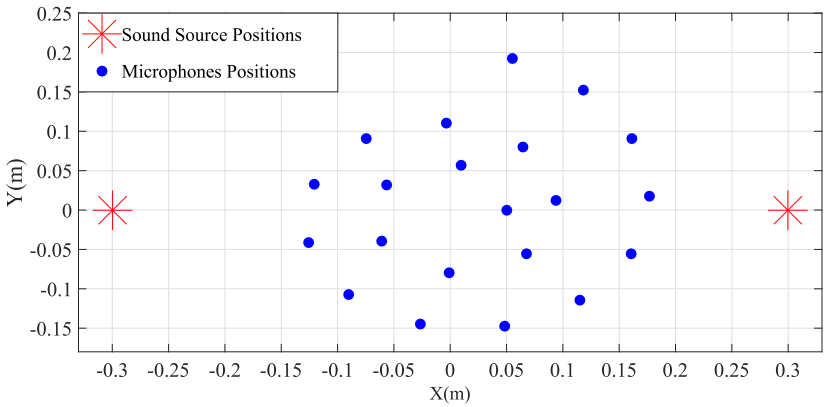

Fig. 2. Positions of microphones and corresponding positions of sound sources.

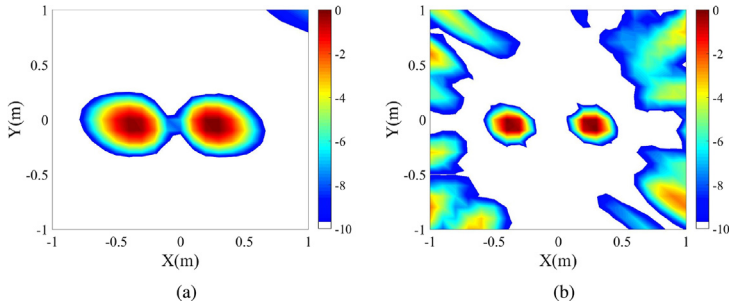

Fig. 3. The beamforming results with the measurements of the prototype array: (a) at 3000 Hz, SNR = 60 dB; (b) at 5000 Hz, SNR = 60 dB.

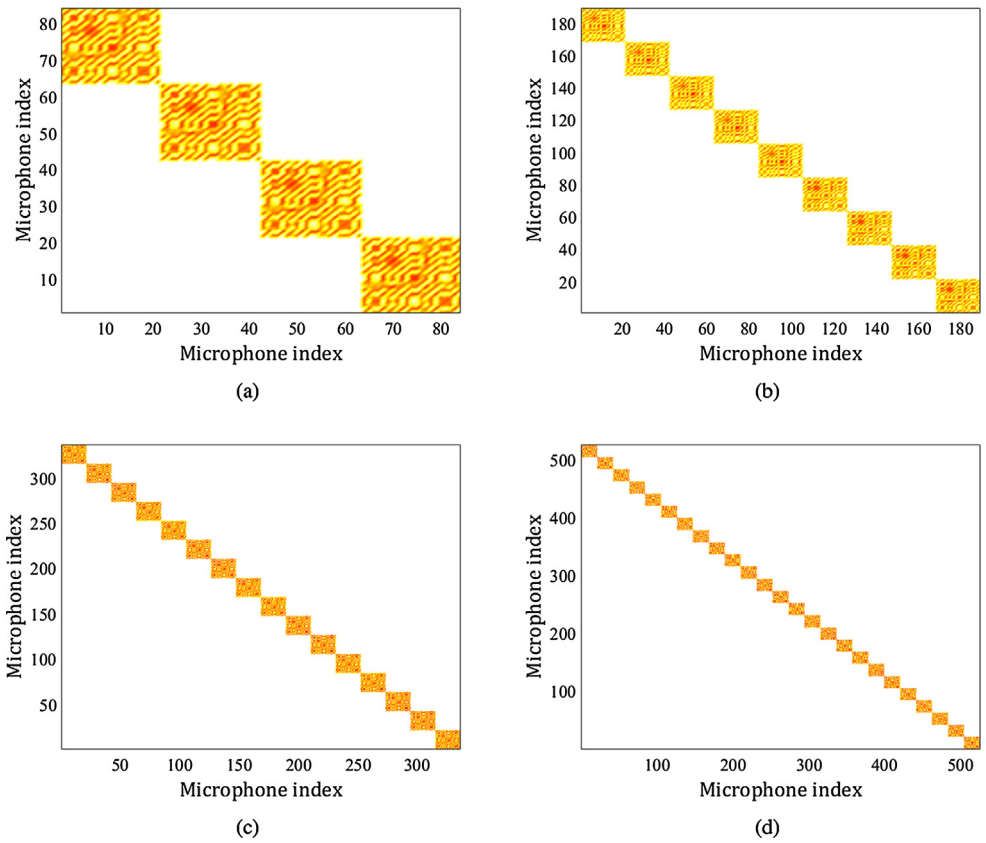

Fig. 4. The data missing cross-spectral matrix of (a) 4 non-synchronous measurements (25% elements are known); (b) 9 non-synchronous measurements (11% elements are known); (c) 16 non-synchronous measurements (6% elements are known); (d) 25 non-synchronous measurements (4% elements are known).

and $\mu = 1/\|\widehat{\mathbf{S}}_{pp}^{m}\|_F$. In ADMM, the parameters are set as follows: maximum iteration step $N_m = 14$ (5 for the case of 4 non-synchronous measurements), stopping criterion $\varepsilon_2 = 5e-3$, gamma $\gamma = 2.6$, regularization parameter $\lambda = 28.5e-3$ and $\mu = 24.5/MP$ (MP is the dimension of $\widehat{\mathbf{S}}_{pp}^{m}$). All the simulations are done by the MATLAB R2015a software on Intel(R) Core (TM) i5-3230M @ 2.60 GHz system with 8 GB-RAM. It is generally accepted that the algorithm comparison is a hard task and there is no theoretical results about the computation speeds of the three methods. Thus, the parameters of each algorithms are chosen as the ones who can achieve the fastest beamforming results, which is empirically the "best we can do" scenario.

The MCE and the CT (computation time) of different methods (FISTA, ALM and ADMM) are shown in Table 1. For the case of 4 non-synchronous measurements, the MCE and CT are the average results for the frequency range from 3000 Hz to 4000 Hz (with a step of 100 Hz). The MCE and CT are the average results for the frequency range from 3000 Hz to 5000 Hz (with a step of 100 Hz) when 9, 16 and 25 non-synchronous measurements are taken. The frequency range is

Table 1
Matrix completion error (MCE) and computation time (CT) of non-synchronous beamforming with three algorithms (FISTA, ALM and ADMM).

	SNR = 10 dB	SNR = 20 dB	SNR = 30 dB	SNR = 60 dB
(MCE,CT)		4 non-synchronous measurements		
FISTA	(12.94%, 0.077s)	(12.16%, 0.064s)	(12.27%, 0.060s)	(12.27%, 0.057s)
ADMM	(21.70%, 0.028s)	(20.34%, 0.024 s)	(19.94%, 0.022s)	(20.17%, 0.020s)
ALM	(79.64%, 0.011s)	(79.72%, 0.009s)	(79.65%, 0.009s)	(79.87%, 0.008s)
(MCE,CT)		9 non-synchronous measurements		
FISTA	(10.92%, 0.61s)	(8.75%, 0.51s)	(8.47%, 0.48s)	(8.41%, 0.49s)
ADMM	(11.57%, 0.37s)	(9.23%, 0.33s)	(8.97%, 0.30s)	(8.89%, 0.28s)
ALM	(91.08%, 0.05s)	(91.03%, 0.04s)	(90.92%, 0.04s)	(90.96%, 0.04s)
(MCE,CT)		16 non-synchronous measurements		
FISTA	(6.65%, 2.20s)	(3.16%, 2.13s)	(2.51%, 2.11s)	(2.41%, 2.11s)
ADMM	(8.98%, 1.37s)	(6.67%, 1.35s)	(6.54%, 1.34s)	(6.40%, 1.37s)
ALM	(94.86%, 0.18s)	(94.83%, 0.17s)	(94.95%, 0.17s)	(94.82%, 0.17s)
(MCE,CT)		25 non-synchronous measurements		
FISTA	(9.22%, 7.77s)	(6.37%, 7.81s)	(6.06%, 7.86s)	(6.03%, 8.11s)
ADMM	(15.55%, 5.13s)	(14.20%, 5.17s)	(13.83%, 6.08s)	(13.91%, 4.71s)
ALM	(96.78%, 0.54s)	(96.69%, 0.54s)	(96.71%, 0.55s)	(96.71%, 0.54s)

extended since the more numbers of non-synchronous measurements are involved (the number of microphones is relatively increased). The simulation results show the MCE of FISTA is usually the lowest one and the CT of ALM is the shortest. The performance of ADMM is in the middle of FISTA and ALM which is a trade-off between the computation time and the matrix completion error. It must also be pointed out that the beamforming results can be correct even if the MCE is quite high. For example, the MCE of ALM is 96.78% when the SNR = 10 dB for the case of 25 non-synchronous measurements. However, the acoustic beamforming results of ALM at 3000 Hz and 5000 Hz are shown in Fig. 5(c) and (d) and the two sources can be well located. It is concluded that the completeness of the cross-spectral matrix plays a more significant role than the estimation accuracy in the beamforming. It should also be noted that the accuracy of the cross-spectral matrix can be improved by setting a large number of iteration N_m for the three algorithms. This parameter is more important for the advanced beamforming methods (e.g., the ClEAN [31] or DAMAS method [32]) which can quantify the sound sources.

The non-synchronous beamforming results of three algorithms (FISTA, ALM and ADMM) with 16 non-synchronous measurements are shown in Fig. 5. The results of FISTA at 3000 Hz and 5000 Hz are shown in Fig. 5(a) and (b); the results of ALM at 3000 Hz and 5000 Hz are respectively shown in Fig. 5(c) and (d); the results of ADMM at 3000 Hz and 5000 Hz are respectively shown in Fig. 5(e) and (f). In fact, the non-synchronous beamforming results at other frequencies (from 3000 Hz to 5000 Hz) are as good as the ones that have been shown here. Thus, the working frequency of the prototype array has been largely extended by the proposed non-synchronous measurements algorithms.

7. An industrial application

An on-site measurement is carried out in the acoustic lab of the SJTU (Shanghai Jiao Tong University). A Buick Regal automobile (2.4L LAF, 2013) is operating at idling. It is well known that the engine and High Pressure Pump (HPP) are two main noise sources in the engine compartment. The general setup of the on-site measurement is shown in Fig. 6 and a dimensioned-diagram with the precise location of the engine relative to the HPP is shown in Fig. 7. It is shown that the size of the engine compartment surface is 85×160 cm in Fig. 7, and a microphone array consisting of 6×8 BSWA MPA201 microphones (1/2 inch condenser microphone) is fixed over the automobile engine as the prototype array for achieving the non-synchronous measurements. The BBM MKII acquisition system is used for the measurement. The prototype array is moved sequentially from position ① to position ⑮ which is illustrated in Fig. 8. The sampling frequency is set to be 25,600 Hz and the total record length of each channel is 15s. The Cartesian coordinate system is used with the origin in the center of the microphone array (it is also the center of the HPP). The x-axis is chosen to be parallel with the short side of vehicle and the y-axis parallel with the long side of the vehicle. The measurement distance is 0.2 m. It is worth noting that this distance is a challenge for the conventional beamforming, and this measurement distance is hard to be extended due to the position limitation of the automobile bonnet.

The direct beamforming results at 2000 Hz and 5680 Hz are shown in Fig. 9. The direct beamforming results at measurement positions ① and ⑧ of 2000 Hz are shown in Fig. 9(a) and (b), and the beamforming results at measurement positions ⑨ and ⑮ of 5680 Hz are shown in Fig. 9(c) and (d). The sound power of beamforming outputs are normalized by the maximum value (displayed with a dB unit), and the dynamic ranges of the beamforming results are set as 15 dB. The position coordinates of each small array are also marked as the black points in the beamforming results. It is observed that the imaging resolution is low and all the sound sources can not be distinguished. The image of the sound sources only in front of the small single array can be obtained within a 15 dB dynamic range, and this is caused by the basic limitation of the number of microphones. Thus, only the partial sound field can be visualized with a small single array. It is known a priori that the engine

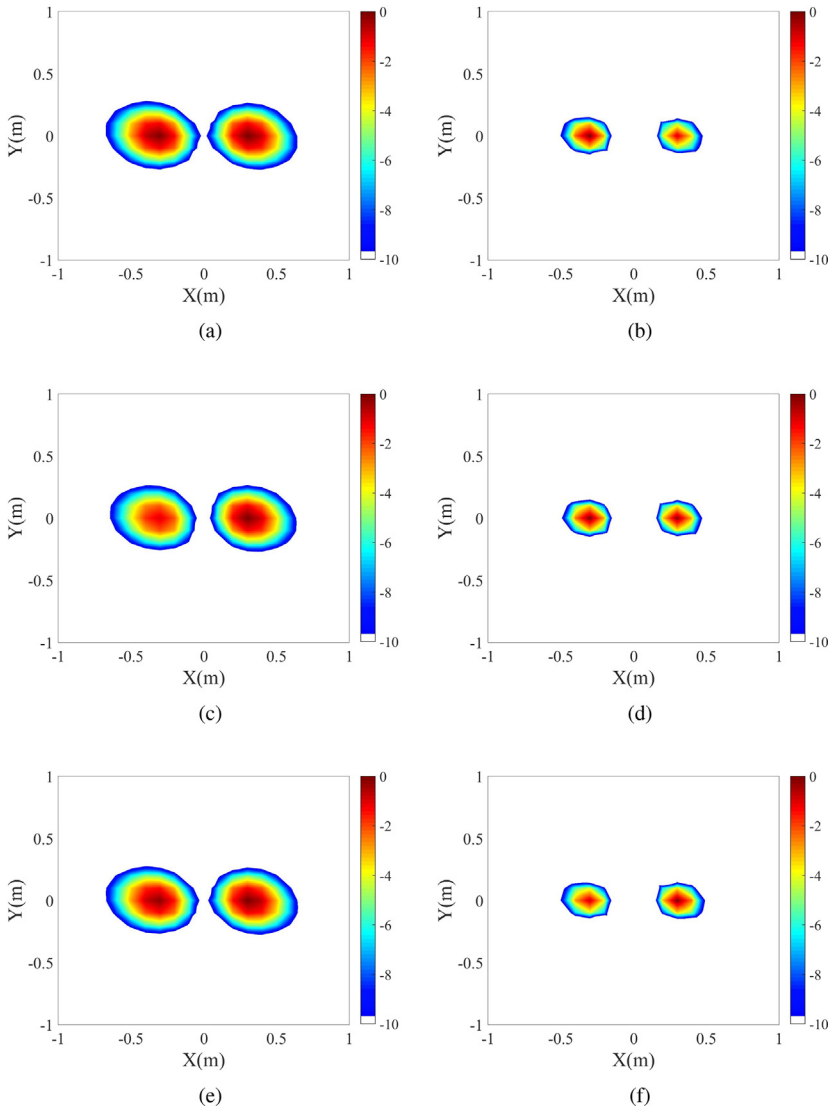

Fig. 5. The non-synchronous beamforming results of three algorithms (FISTA, ALM and ADMM) with 16 non-synchronous measurements: (a) FISTA (SNR = 10 dB, 3000 Hz); (b) FISTA (SNR = 10 dB, 5000 Hz); (c) ALM (SNR = 10 dB, 3000 Hz); (d) ALM (SNR = 10 dB, 5000 Hz); (e) ADMM (SNR = 10 dB, 3000 Hz); (f) ADMM (SNR = 10 dB, 5000 Hz).

noise dominates at 2000 Hz and the HPP noise is strong at 5680 Hz. However, the imaging results of a single measurement can not verify this a priori information about the sound sources.

In order to have a global view of the sound sources, more microphones are required. The purpose of non-synchronous microphone array measurements is making use of all the measurements at positions from ① to ⑮. The data missing cross-spectral matrix is 720×720 (48 microphones are moved 15 times and the total elements of the cross-spectral matrix are 518400), and only 34,560 elements of the cross-spectral matrix are known (only 7% elements are known). The FISTA, ALM and ADMM are implemented for the non-synchronous measurements. It is noted that the FISTA have already been validated in the laboratory [16]. Thus the results of FISTA is considered as the ground truth in this measurement (the iteration number in the algorithm is set to be high enough to guarantee the ground truth results). The parameters of FISTA are chosen as follows: maximum iteration for each regularization step $N_m = 5$, stopping criterion $SC = 1e-2$, initial regularization parameter $\lambda_0 = \|\hat{\mathbf{S}}_{pp}^m\|_F$, final regularization parameter $\lambda_d = 10^{-16}\lambda_0$ and step size $\mu = 1.2$. The parameters for ALM are chosen as follows: maximum iteration $N_m = 50$, stopping criterion $\varepsilon_1 = 1e-2$, and $\mu = 1/\|\hat{\mathbf{S}}_{pp}^m\|_F$. In ADMM, the parameters are set as follows: maximum iteration $N_m = 50$, stopping criterion $\varepsilon_2 = 5e-3, \gamma = 2.6, \lambda = 28.5e-3$ and $\mu = 24.5/720$.

The imaging results by non-synchronous microphone array measurements at 2000 Hz of FISTA, ALM, and ADMM methods are shown in Fig. 10(a)–(c). The computational time of FISTA, ALM and ADMM at 2000 Hz are respectively 168.0168 s,

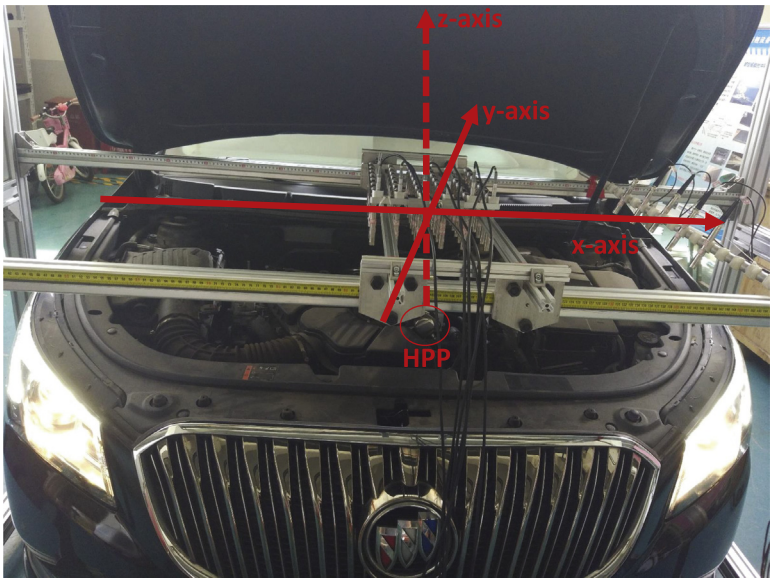

Fig. 6. Experimental setup: a microphone array support assembled over the engine compartment of a Buick Regal.

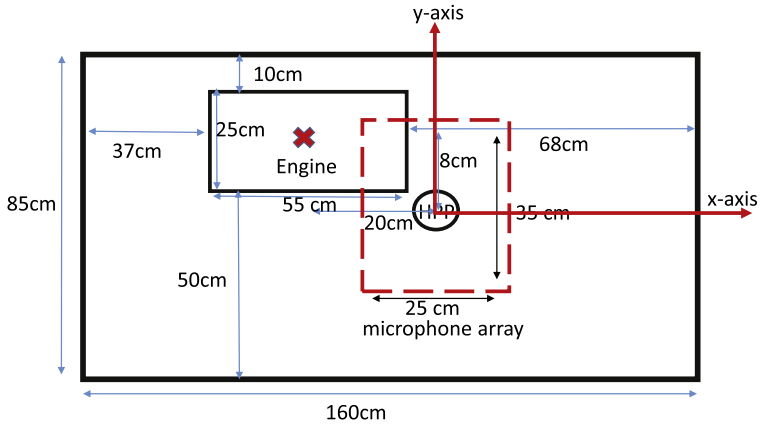

Fig. 7. A dimensioned-diagram shows the precise location of the engine relative to the HPP in the engine compartment.

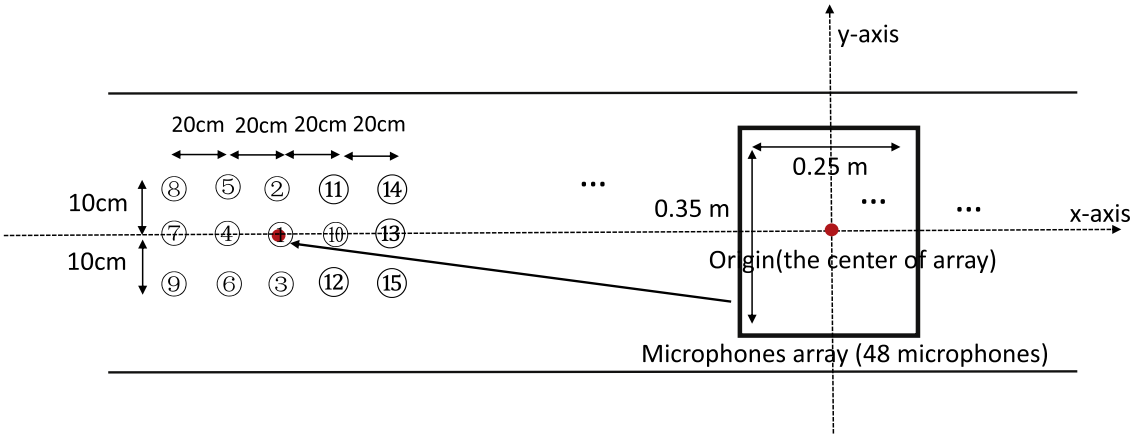

Fig. 8. Setup parameters of non-synchronous measurements.

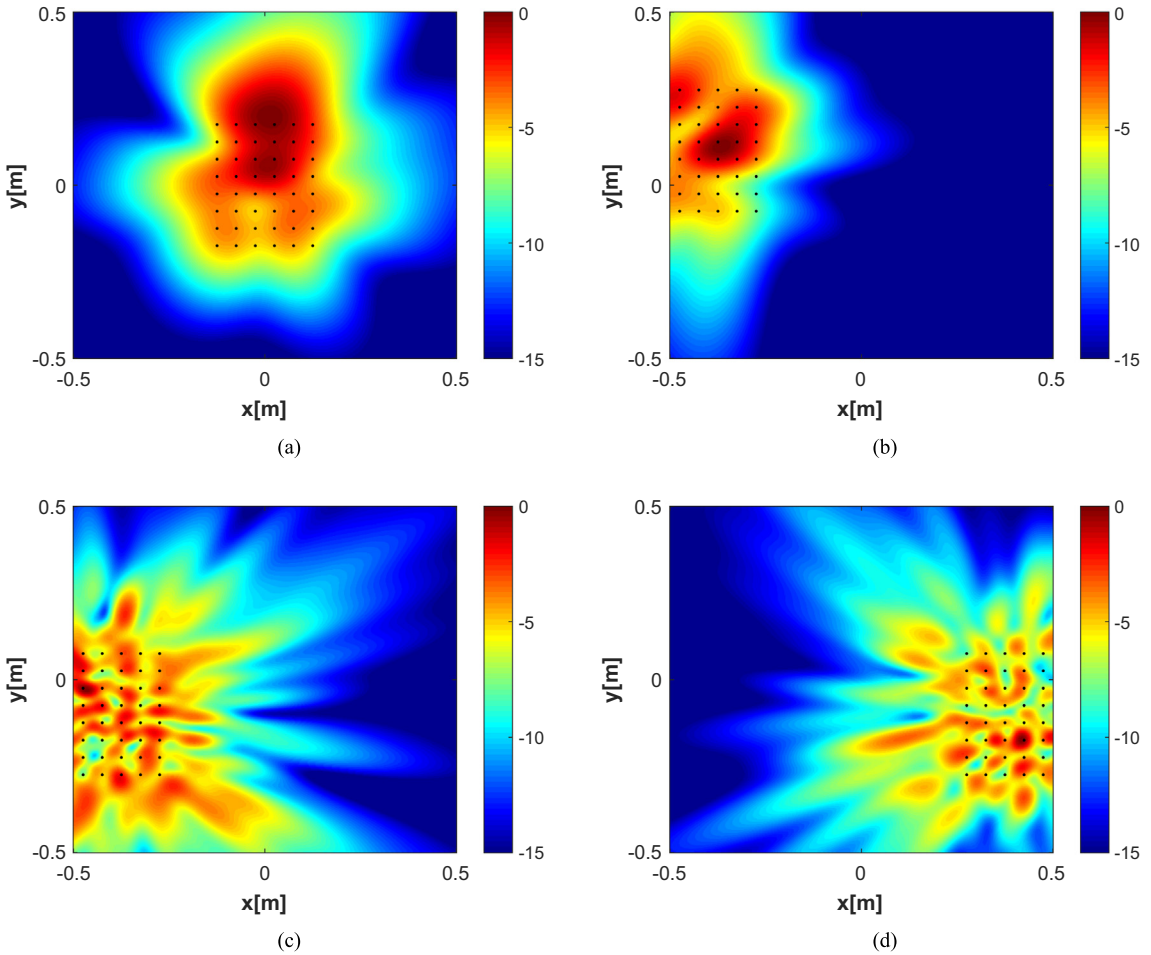

Fig. 9. Beamforming results by direct conventional beamforming at (a) the 1st position (2000 Hz), (b) the 8th position (2000 Hz), (c) the 9th position (5680 Hz), and (d) the 15th position (5680 Hz). The beamforming results are normalized by the maximum beamforming output and shown in dB unit; the dynamic range is 15 dB.

3.4319 s and 16.9813 s. The images with higher resolution and dynamic range as compared with the direct beamforming are shown in Fig. 10. It is observed that the dominant energy is radiated from the engine at this frequency and the HPP noise source looks very weak. The observation is in accordance with our a priori information that the engine noise dominates at low frequencies.

The imaging results by non-synchronous measurements at 5680 Hz of FISTA, ALM, and ADMM methods are shown in Fig. 11(a)–(c). The computational time of FISTA, ALM and ADMM at 5680 Hz are respectively 160.1995s, 3.1960s and

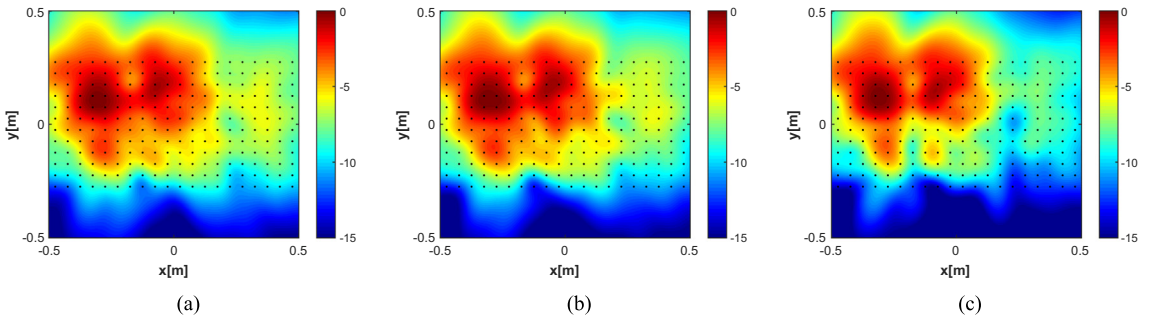

Fig. 10. Beamforming results by non-synchronous microphone array measurements at 2000 Hz of (a) FISTA, (b) ALM, and (c) ADMM method. The beamforming results are normalized by the maximum beamforming output and shown in dB unit; the dynamic range is 15 dB.

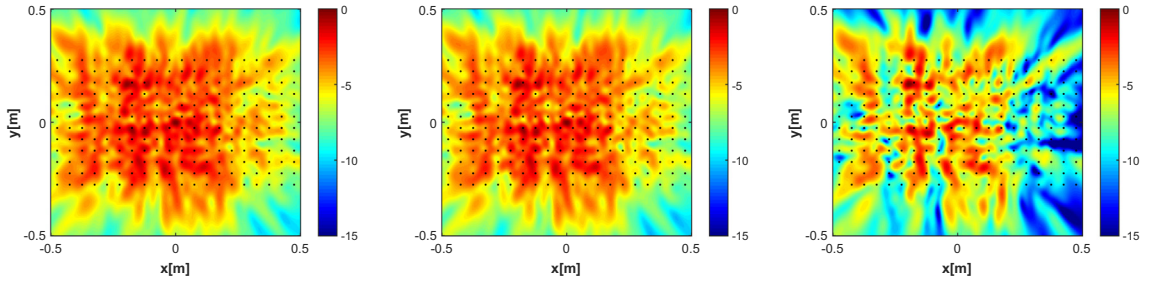

Fig. 11. Beamforming results by non-synchronous microphone array measurements at 5680 Hz of (a) FISTA, (b) ALM, and (c) ADMM method. The beamforming results are normalized by the maximum beamforming output and shown in dB unit; the dynamic range is 15 dB.

15.5193s. In this case, the HPP noise source has already appeared in the imaging results of ALM and ADMM (it is shown in the central position of the coordinates). The sound field is much more complex in high frequencies since both the engine and HPP radiates the strong noises. The global image is obtained by the non-synchronous microphone array measurements, and all the microphones are marked with black points in the beamforming results. The non-synchronous measurements virtually utilize all the microphones since the phase information has been recovered by the algorithm. It is concluded that the proposed ALM and ADMM methods almost achieve similar results with the benchmark results of FISTA and the implementation of the proposed methods are much rapid. It seems that the computation time is no longer a problem for the on-site measurements, which is accelerated by the proposed methods. The engine compartment is the first case to apply, and it is shown the potential to be further used for the imaging of large sound sources. The interesting part is that the global image with a higher dynamic range of the large noise sources can be fast obtained, which is more difficult to be achieved by the conventional array measurements.

8. Conclusion

Since the resolution of acoustic beamforming is limited due to the number of microphones, it usually requires a trade-off between the aperture of an array and the spatial separation of the microphones during the array design. Thus, it is still a challenge to apply the beamforming in imaging of large sound sources (or very small ones). The non-synchronous measurements beamforming is investigated in this paper, where a large array and high microphone density array can be virtually formed by moving a prototype array. It is formulated as a cross-spectral matrix completion problem which is solved by minimizing the nuclear norm of a cross-spectral matrix subject to measurements fitting, Hermitian symmetry, and spatial continuity of the sound field. Then the matrix completion problem caused by non-synchronous measurements is implemented with the ALM and ADMM algorithm. The proposed methods have been extensively analyzed with the simulation, and an application of the proposed methods in a vehicle is also given. It is shown that the data missing cross-spectral matrix of 15 non-synchronous measurements for a given frequency can be completed only in a few seconds. Thus, the proposed method has the potential to be further applied in the imaging of large objects of sound radiation (i.e.,the ship, helicopter and submarine).

Acknowledgements

This work was supported by National Natural Science Foundation of China (Grant No. 11704248, 51835008, 11574212), Open Fund of the Key Laboratory of Aerodynamic Noise Control (ANCL20180302) and Startup Fund for Youngman Research at SJTU (SFYR at SJTU) (18X100040061).

Appendix A. The derivation of main iteration step of Algorithm 2

It is well known that the low rank approximation $\mathbf{X}$ from a matrix $\mathbf{Z}$ can be obtained by the shrink operator $\text{shrink}(\mathbf{Z},\tau)$ which obeys $\text{shrink}(\mathbf{Z},\tau)=\underset{\mathbf{X}}{\text{argmin}}\ \frac{1}{2}\|\mathbf{X}-\mathbf{Z}\|_F^2+\tau\|\mathbf{X}\|_*$, where τ is a regularization parameter (see the Theorem 2.1 of Ref. [33]) and this operator is also called singular value soft-thresholding operator which can be applied for a real or complex matrix [34,35]. Then the augmented Lagrange function Eq. (12) can be solved as follows.

$$\begin{aligned}\tilde{\mathbf{S}} &= \underset{\mathbf{S}}{\text{argmin}}\ \|\mathbf{S}\|_* + \left\langle \mathbf{Y}, \widehat{\mathbf{S}}_{pp}^m - \mathbf{S} - \mathbf{E}\right\rangle + \frac{\mu}{2}\|\widehat{\mathbf{S}}_{pp}^m - \mathbf{S} - \mathbf{E}\|_F^2 = \underset{\mathbf{S}}{\text{argmin}}\|\mathbf{S}\|_* + \frac{\mu}{2}\|\widehat{\mathbf{S}}_{pp}^m - \mathbf{S} - \mathbf{E} + \mu^{-1}\mathbf{Y}\|_F^2 \\ &= \text{shrink}\left(\widehat{\mathbf{S}}_{pp}^m - \mathbf{E} + \mu^{-1}\mathbf{Y}, \mu\right) = \mathbf{U}\text{diag}\left(\max\{\boldsymbol{\sigma} - \boldsymbol{\mu}, \mathbf{0}\}\right)\mathbf{U}^H, \end{aligned} \tag{A.1}$$

where $\mathbf{U}$ and $\mathrm{diag}(\boldsymbol{\sigma})$ are respectively the eigenvector matrix and eigenvalue matrix of Eigenvalue Decomposition of matrix $\widehat{\mathbf{S}}_{pp}^{m}-\mathbf{E}+\mu^{-1}\mathbf{Y}$. The constraint $\|\boldsymbol{\Psi}\mathbf{S}\boldsymbol{\Psi}^{H}-\mathbf{S}\|_{F}\leqslant\varepsilon$ and $\mathcal{A}(\mathbf{E})=0$ should be enforced by setting $\mathbf{S}_{k+1}=\boldsymbol{\Psi}\tilde{\mathbf{S}}_{k}\boldsymbol{\Psi}^{H}$ and $\mathbf{E}_{k+1}=\bar{\mathcal{A}}\left(\widehat{\mathbf{S}}_{pp}^{m}-\mathbf{S}_{k+1}+\mu^{-1}\mathbf{Y}_{k}\right)$ in each iteration.The Lagrange multiplier $\mathbf{Y}$ can be updated by $\mathbf{Y}_{k+1}=\mathbf{Y}_{k}+\mu\left(\widehat{\mathbf{S}}_{pp}^{m}-\mathbf{S}_{k+1}-\mathbf{E}_{k+1}\right)$ according to Algorithm 2.

Appendix B. The derivation of main iteration step of Algorithm 4

Similar with the low rank approximation theorem of appendix A, The Eq. (22) can be solved by the following derivations.

$$\begin{aligned}\tilde{\mathbf{S}}_{k} &= \underset{\mathbf{S}}{\operatorname{argmin}}\lambda\|\mathbf{S}\|_{*}+\frac{1}{2}\|\mathcal{A}(\mathbf{M}_{k})-\widehat{\mathbf{S}}_{pp}^{m}\|_{F}^{2}+\langle\mathbf{Y}_{k},\mathbf{S}-\mathbf{M}_{k}\rangle+\frac{\mu}{2}\|\mathbf{S}-\mathbf{M}_{k}\|_{F}^{2}=\underset{\mathbf{S}}{\operatorname{argmin}}\lambda\|\mathbf{S}\|_{*}+\frac{\mu}{2}\|\mathbf{S}-\mathbf{M}_{k}+(1/\mu)\mathbf{Y}_{k}\|_{F}^{2}\\ &=\mathrm{shrink}(\mathbf{M}_{k}-(1/\mu)\mathbf{Y}_{k},\lambda/\mu)=\mathbf{U}_{k}\mathrm{diag}\left(\max\{\boldsymbol{\omega}_{k}-\boldsymbol{\lambda}/\boldsymbol{\mu},\mathbf{0}\}\right)\mathbf{U}_{k}^{H},\end{aligned}\tag{B.1}$$

where $\mathbf{U}_{k}$ and $\mathrm{diag}(\boldsymbol{\omega}_{k})$ are respectively the eigenvector matrix and eigenvalue matrix of Eigenvalue Decomposition of matrix $\mathbf{M}_{k}-(1/\mu)\mathbf{Y}_{k}$. The constraint $\|\boldsymbol{\Psi}\mathbf{S}\boldsymbol{\Psi}^{H}-\mathbf{S}\|_{F}\leqslant\varepsilon$ should also be enforced by setting $\mathbf{S}_{k+1}=\boldsymbol{\Psi}\tilde{\mathbf{S}}_{k}\boldsymbol{\Psi}^{H}$. The Eq. (23) can be written as

$$\mathbf{M}_{k+1}=\underset{\mathbf{M}}{\operatorname{argmin}}\quad\frac{1}{2}\|\mathcal{A}(\mathbf{M})-\widehat{\mathbf{S}}_{pp}^{m}\|_{F}^{2}+\frac{\mu}{2}\|\mathbf{M}-(1/\mu)\mathbf{Y}_{k}-\mathbf{S}_{k+1}\|_{F}^{2}.\tag{B.2}$$

Then, Eq. (B.2) can be separated into two parts, $\mathcal{A}(\mathbf{M}_{k+1})$ and $\bar{\mathcal{A}}(\mathbf{M}_{k+1})$ respectively:

$$\begin{aligned}\mathcal{A}(\mathbf{M}_{k+1}) &= \underset{\mathcal{A}(\mathbf{M})}{\operatorname{argmin}}\quad\frac{1}{2}\|\mathcal{A}(\mathbf{M})-\mathcal{A}\left(\widehat{\mathbf{S}}_{pp}^{m}\right)\|_{F}^{2}+\frac{\mu}{2}\|\mathcal{A}(\mathbf{M})-(1/\mu)\mathcal{A}(\mathbf{Y}_{k})-\mathcal{A}(\mathbf{S}_{k+1})\|_{F}^{2}\\ &= \underset{\mathcal{A}(\mathbf{M})}{\operatorname{argmin}}\quad\frac{\mu}{2}\|(1/\mu)\mathcal{A}(\mathbf{M})-(1/\mu)\mathcal{A}\left(\widehat{\mathbf{S}}_{pp}^{m}\right)-\mathcal{A}(\mathbf{S}_{k+1})+\mathcal{A}(\mathbf{M})-(1/\mu)\mathcal{A}(\mathbf{Y}_{k})\|_{F}^{2}\\ &= \underset{\mathcal{A}(\mathbf{M})}{\operatorname{argmin}}\quad\frac{\mu}{2}\|\frac{\mu+1}{\mu}\mathcal{A}(\mathbf{M})-(1/\mu)\mathcal{A}\left(\widehat{\mathbf{S}}_{pp}^{m}\right)-\mathcal{A}(\mathbf{S}_{k+1})-(1/\mu)\mathcal{A}(\mathbf{Y}_{k})\|_{F}^{2}\\ &= \underset{\mathcal{A}(\mathbf{M})}{\operatorname{argmin}}\quad\frac{\mu}{2}\|\frac{\mu+1}{\mu}\mathcal{A}(\mathbf{M})-\frac{1}{\mu}\mathcal{A}\left(\widehat{\mathbf{S}}_{pp}^{m}+\mu\mathbf{S}_{k+1}+\mathbf{Y}_{k}\right)\|_{F}^{2};\end{aligned}\tag{B.3}$$

$$\bar{\mathcal{A}}(\mathbf{M}_{k+1})=\underset{\bar{\mathcal{A}}(\mathbf{M})}{\operatorname{argmin}}\quad\frac{\mu}{2}\|\bar{\mathcal{A}}(\mathbf{M})-\bar{\mathcal{A}}(\mathbf{S}_{k+1})-(1/\mu)\bar{\mathcal{A}}(\mathbf{Y}_{k})\|_{F}^{2}=\underset{\bar{\mathcal{A}}(\mathbf{M})}{\operatorname{argmin}}\quad\frac{\mu}{2}\|\bar{\mathcal{A}}(\mathbf{M})-\bar{\mathcal{A}}(\mathbf{S}_{k+1}+(1/\mu)\mathbf{Y}_{k})\|_{F}^{2}.\tag{B.4}$$

Therefore, Eqs. (B.3) and (B.4) can be easily solved by the following equations

$$\mathcal{A}(\mathbf{M}_{k+1})=\frac{1}{\mu+1}\mathcal{A}\left(\widehat{\mathbf{S}}_{pp}^{m}+\mu\mathbf{S}_{k+1}+\mathbf{Y}_{k}\right);\tag{B.5}$$

$$\bar{\mathcal{A}}(\mathbf{M}_{k+1})=\bar{\mathcal{A}}(\mathbf{S}_{k+1}+(1/\mu)\mathbf{Y}_{k}).\tag{B.6}$$

Finally, the Lagrange multiplier $\mathbf{Y}$ can also be updated by $\mathbf{Y}_{k+1}=\mathbf{Y}_{k}+\gamma\mu(\mathbf{S}_{k+1}-\mathbf{M}_{k+1})$ according to the iterations in Algorithm 4.

References

[1] W. Lu, W. Jiang, G. Yuan, L. Yan, A gearbox fault diagnosis scheme based on near-field acoustic holography and spatial distribution features of sound field, J. Sound Vib. 332 (10) (2013) 2593–2610.
[2] C. Pézerat, Q. Leclère, N. Totaro, M. Pachebat, Identification of vibration excitations from acoustic measurements using near field acoustic holography and the force analysis technique, J. Sound Vib. 326 (3–5) (2009) 540–556.
[3] M. Lee, J.S. Bolton, Source characterization of a subsonic jet by using near-field acoustical holography, J. Acoust. Soc. Am. 121 (2) (2007) 967–977.
[4] R.P. Dougherty, Beamforming for aircraft noise measurements, J. Acoust. Soc. Am. 114 (4) (2003) 2339.
[5] Q. Leclre, A. Pereira, C. Bailly, J. Antoni, C. Picard, A unified formalism for acoustic imaging based on microphone array measurements, Int. J. Aeroacoust. 16 (4–5) (2017) 431–456.
[6] C.J. Bahr, W.M. Humphreys, D. Ernst, T. Ahlefeldt, C. Spehr, A. Pereira, Q. Leclere, C. Picard, R. Porteous, D. Moreau, J. Fischer, C.J. Doolan, A Comparison of Microphone Phased Array Methods Applied to the Study of Airframe Noise in Wind Tunnel Testing, AIAA, Denver, United States, 2017.
[7] E.G. Williams, Fourier Acoustics: Sound Radiation and Nearfield Acoustical Holography, Academic Press, 1999.
[8] J.-C. Pascal, S. Paillasseur, J.-H. Thomas, J.-F. Li, Patch near-field acoustic holography: regularized extension and statistically optimized methods, J. Acoust. Soc. Am. 126 (3) (2009) 1264–1268.
[9] J. Hald, Basic theory and properties of statistically optimized near-field acoustical holography, J. Acoust. Soc. Am. 125 (4) (2009) 2105–2120.
[10] L. Yu, Acoustical Source Reconstruction from Non-synchronous Sequential Measurements, INSA de Lyon, 2015 (Ph.D. thesis).
[11] S. Barre, C. Puhle, Acoustic sources distribution reconstruction from non-synchronous sound pressure measurements, in: INTER-NOISE 2017, the 46th International Congress and Exposition on Noise Control Engineering, Leuven, Belgium, 2017, p. CDROM..
[12] L.K. Wachter, J. Ocker, D. Dobler, C. Puhle, G. Herold, Investigations on beamforming in the wind tunnel using multiple microphone array measurements, in: 7th berlin beamforming conference. 5th march, Berlin, Germany., 2018..

[13] T. Loyau, J.-C. Pascal, P. Gaillard, Broadband acoustic holography reconstruction from acoustic intensity measurements. i: Principle of the method, J. Acoust. Soc. Am. 84 (5) (1988) 1744–1750.
[14] C.-X. Bi, W.-Q. Jing, Y.-B. Zhang, Broadband acoustic holography from intensity measurements with a three-dimensional pressure-velocity probe, J. Acoust. Soc. Am. 138 (5) (2015) 2929–2936.
[15] L. Yu, J. Antoni, Q. Leclère, Spectral matrix completion by cyclic projection and application to sound source reconstruction from non-synchronous measurements, J. Sound Vib. 372 (2016) 31–49.
[16] L. Yu, J. Antoni, Q. Leclere, W. Jiang, Acoustical source reconstruction from non-synchronous sequential measurements by fast iterative shrinkage thresholding algorithm, J. Sound Vib. 408 (2017) 351–367.
[17] A. Nejade, Reference-less acoustic holography techniques based on sound intensity, J. Sound Vib. 333 (16) (2014) 3598–3608.
[18] S. Yoon, P. Nelson, A method for the efficient construction of acoustic pressure cross-spectral matrices, J. Sound Vibr. 233 (5) (2000) 897–920.
[19] L. Yu, W. Jiang, J. Antoni, Q. Leclere, H. Wu, Acoustical beamforming using non-synchronous microphone array measurements, Berlin Beamforming Conference (2018).
[20] S. Xiang, W. Jiang, H. Jiang, J. Gao, Reconstructing the normal velocities of acoustic sources in noisy environments using a rigid microphone array, J. Acoust. Soc. Am. 140 (3) (2016) 2082–2090.
[21] J. Antoni, A bayesian approach to sound source reconstruction: optimal basis, regularization, and focusing, J. Acoust. Soc. Am. 131 (4) (2012) 2873–2890.
[22] P. Welch, The use of fast fourier transform for the estimation of power spectra: a method based on time averaging over short, modified periodograms, IEEE Trans. Audio Electroacoust. (1967) 70–73.
[23] D.P. Bertsekas, Constrained Optimization and Lagrange Multiplier Methods, AP, 1982.
[24] Z. Lin, M. Chen, Y. Ma, The augmented lagrange multiplier method for exact recovery of corrupted low-rank matrices, arXiv preprint arXiv:1009.5055..
[25] F. Xu, P. Pan, A new algorithm for positive semidefinite matrix completion, J. Appl. Math. (2016).
[26] E. Ghadimi, A. Teixeira, I. Shames, M. Johansson, Optimal parameter selection for the alternating direction method of multipliers (ADMM): quadratic problems, IEEE Trans. Autom. Control 60 (3) (2015) 644–658.
[27] R. Nishihara, L. Lessard, B. Recht, A. Packard, M.I. Jordan, A general analysis of the convergence of admm, in: Proceedings of the 32Nd International Conference on International Conference on Machine Learning – Volume 37, 2015, pp. 343–352, ICML'15, JMLR.org.
[28] X. Yuan, J. Yang, Sparse and low rank matrix decomposition via alternating direction method, Pacific J. Optim. 9 (1) (2009).
[29] M.R. Bai, J.-G. Ih, J. Benesty, Acoustic Array Systems: Theory, Implementation, and Application, John Wiley & Sons, 2013.
[30] T. Mueller, C. Allen, W. Blake, R. Dougherty, D. Lynch, P. Soderman, J. Underbrink, Aeroacoustic Measurements, Springer, Engineering online library, 2002.
[31] P. Sijtsma, Clean based on spatial source coherence, Int. J. Aeroacoust. 6 (4) (2007) 357–374.
[32] T.F. Brooks, W.M. Humphreys, A deconvolution approach for the mapping of acoustic sources (damas) determined from phased microphone arrays, J. Sound Vib. 294 (4) (2006) 856–879.
[33] J.-F. Cai, E.J. Candès, Z. Shen, A singular value thresholding algorithm for matrix completion, SIAM J. Optim. 20 (4) (2010) 1956–1982.
[34] M. Weimin, Matrix completion models with fixed basis coefficients and rank regularized problems with hard constraints (Ph.D. thesis), 2013..
[35] T.-S.T. Chan, Y.-H. Yang, Complex and quaternionic principal component pursuit and its application to audio separation, IEEE Signal Process. Lett. 23 (2) (2016) 287–291.